AIP | Applied Physics Letters

# Generation and recombination rates at ZnTe:O intermediate band states

Weiming Wang, Albert S. Lin, Jamie D. Phillips, and Wyatt K. Metzger

Citation: Appl. Phys. Lett. **95**, 261107 (2009); doi: 10.1063/1.3274131
View online: http://dx.doi.org/10.1063/1.3274131
View Table of Contents: http://apl.aip.org/resource/1/APPLAB/v95/i26
Published by the American Institute of Physics.

# Generation and recombination rates at ZnTe:O intermediate band states

Weiming Wang (王伟明),[1,a] Albert S. Lin,[1] Jamie D. Phillips,[1] and Wyatt K. Metzger[2]
[1]*Department of Electrical Engineering and Computer Science, The University of Michigan, Ann Arbor, Michigan 48109-2122, USA*
[2]*National Renewable Energy Laboratory, Golden, Colorado 80401, USA*

(Received 3 November 2009; accepted 23 November 2009; published online 30 December 2009)

Carrier generation and recombination processes of ZnTeO thin films are studied by time-resolved photoluminescence, where carrier lifetimes at oxygen states and the conduction band are inferred to be $>1$ $\mu$s and $<100$ ps, respectively. The radiative recombination coefficient for optical transitions from oxygen states to the valence band is extracted to be $1.2\times10^{-10}$ $cm^3$ $sec^{-1}$ based on the excitation dependence of decay time constants. Rate equation analysis further suggests an increase in electron lifetime at the conduction band as oxygen states occupation is critical in achieving high conversion efficiency for solar cells based on multiphoton processes in these materials. © *2009 American Institute of Physics*. [doi:10.1063/1.3274131]

Solar cells based on absorber materials with intermediate electron states within the band gap have been proposed in order to improve conversion efficiency using lower energy optical transitions via multiple photon emission. These devices, typically referred to as intermediate band solar cells (IBSCs), are based on a single p-n junction with a predicted theoretical efficiency of 63%,[1] as high as the theoretical efficiency of a triple junction solar cell.[2] Intermediate band absorber materials based on quantum wells,[3] quantum dots,[4–9] dilute semiconductor alloys,[10–12] and deep level impurities[13,14] have been studied experimentally. Subband gap absorption has been observed via IB states in these structures, though an understanding of the dynamic carrier recombination and generation processes via the IB have not been studied in detail despite their major importance in determining conversion efficiency.[15] Theoretical conversion efficiency predictions for IBSC are based on assumptions of long carrier lifetimes in both the intermediate band states and conduction band (CB), which do not necessarily hold true in practice due to fast nonradiative or radiative recombination processes. The incorporation of oxygen into ZnTe results in electronic states within the band gap with highly radiative properties, long carrier lifetimes,[16] and has been proposed as a candidate material system for IBSC devices. The energy band diagram for ZnTe:O and associated optical transitions are shown in Fig. 1(a). The small peaks in the subband gap luminescence in the ZnTe:NO sample suggest phonon emission and a strong Huang–Rhys factor, the latter occurs when there is a strong coupling of the transition to the lattice (e.g., when an electron leaves a given site the lattice is strongly perturbed) and is often associated with donor-acceptor pair transitions and point defects, rather than a band. Similar peaks appear in the ZnTe:O sample. In this letter, carrier lifetimes in ZnTe:O are measured and applied to a rate equation model to assess generation-recombination processes relevant for IBSC.

ZnTe:O samples were grown on GaAs(100) substrates by molecular beam epitaxy using solid source effusion cells for Zn and Te, and an electron cyclotron resonance plasma cell for oxygen and nitrogen incorporation. The nominal thickness of ZnTe samples is 2 $\mu$m, with further details on material growth reported previously.[17] Three samples were studied for comparison with varying oxygen and nitrogen incorporation, as shown in Table I. Hall-effect measurements indicate that samples doped with nitrogen at a flow rate of 0.8 sccm exhibit p-type conduction with a carrier concentration of $10^{19}$ $cm^{-3}$. The sample doped with oxygen only demonstrated p-type conduction with a background concentration of $10^{15}$ $cm^{-3}$, attributable to native zinc vacancies.[18] Oxygen incorporates as a substitutional impurity in the tellurium site ($O_{Te}$) under these growth conditions, resulting in isoelectronic states in ZnTe.[17] The density of $O_{Te}$ state is estimated from the absorption coefficient based on the relation $N_O(cm^{-3})=10^{16}\alpha_O(cm^{-1})$ (Ref. 16), where $N_O$ is the density of $O_{Te}$ state and $\alpha_O$ is the optical absorption coefficient of transition between the valence band (VB) and $O_{Te}$ states. The optical absorption coefficient has been characterized previously on ZnTe:O/sapphire structure.[17] For oxygen flow rates of 0.08 and 0.02 sccm, the absorption coefficients are approximately $10^3$ and $10^2$ $cm^{-3}$ resulting in oxygen concentration of $10^{19}$ and $10^{18}$ $cm^{-3}$, respectively. However, the oxygen doping concentration may be higher than these values because of high possibility of forming oxygen interstitial in ZnTe.[19] Photoluminescence (PL) spectra were measured at room temperature using a He-Cd laser at 325 nm, monochrometer, and lock-in detection. Time-resolved photoluminescence (TRPL) measurements were also conducted at

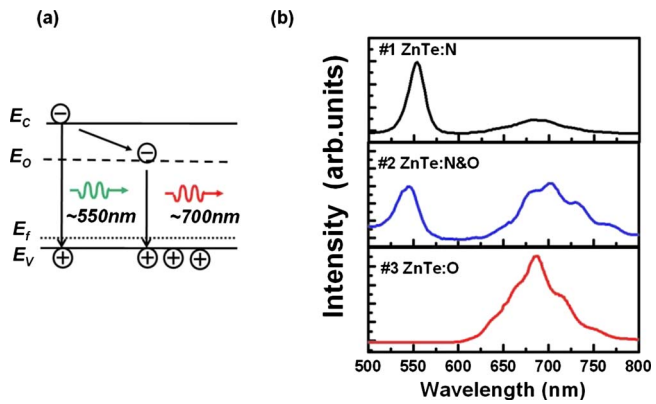


FIG. 1. (Color online) (a) Schematic energy band diagram for ZnTe:O and illustration of optical transitions and (b) room temperature PL spectra for ZnTe:N, ZnTe:NO, and ZnTe:O samples.

[a]Electronic mail: umwwm@umich.edu.

 

TABLE I. Doping concentration, TRPL measurement conditions for 550 and 700 nm emissions, and measured lifetimes of ZnTe:N, ZnTe:NO, and ZnTe:O samples.

| | ZnTe:N | ZnTe:NO | ZnTe:O |
|---|---|---|---|
| Hole concentration ($cm^{-3}$) | $10^{19}$ | $\sim 10^{19}$ | $\sim 10^{15}$ |
| $O_{Te}$ concentration ($cm^3$) | ⋯ | $\sim 10^{19}$ | $\sim 10^{18}$ |
| Lifetime for CB electrons (ps) | <100 | <100 | <100 |
| Lifetime for O-state electrons | 990 ps | 160 ps | 0.6–4 $\mu$s |

room temperature using excitation at 400 nm and detection at 550 and 700 nm.

PL spectra for the three ZnTe samples with differing oxygen/nitrogen incorporation are shown in Fig. 1(b). The ZnTe:N sample demonstrates emission predominantly at 550 nm (2.25 eV), corresponding to the CB to the VB transition for ZnTe. The ZnTe:NO sample also shows a conduction to VB transition at 550 nm, as well as a broad peak centered near 700 nm corresponding to transitions from oxygen states (intermediate band, IB) to VB.[20] For the ZnTe:O sample doped exclusively with oxygen, however, only the transition from the oxygen states to the VB is observed. The lack of a clear conduction-valence band transition for the ZnTe:O sample is attributed to fast electron relaxation from CB to oxygen states, as described in more detail in the following discussion section. Time-resolved PL data for the three samples are summarized in Table I, with a representative scan at 700 nm shown in Fig. 2. For both ZnTe:N and ZnTe:NO, the PL decay for the emission peaks at 550 nm are equivalent to the system response of the TRPL setup. This indicates that the carrier lifetime for electrons in the CB is less than 100 ps. The emission at 700 nm can be fit with a biexponential function with two time constants, where the PL intensity follows the relation $A_0+A_1\exp(-t/\tau_1)+A_2\exp(-t/\tau_2)$. For the ZnTe:O sample, long decay times exceeding 1 $\mu$s are observed at low injection levels. In contrast to the ZnTe:N and ZnTe:NO samples, the decay time constant for recombination in the ZnTe:O sample exhibits a dependence on injection level, as illustrated in Fig. 3(a) with extracted time constants shown in Fig. 3(b).

The variations in PL and TRPL behavior in the ZnTe samples with varying nitrogen and oxygen content may be attributed to carrier concentration and density of oxygen electronic states, as described in the following analysis. The ZnTe:N sample exhibits a short recombination time attribute

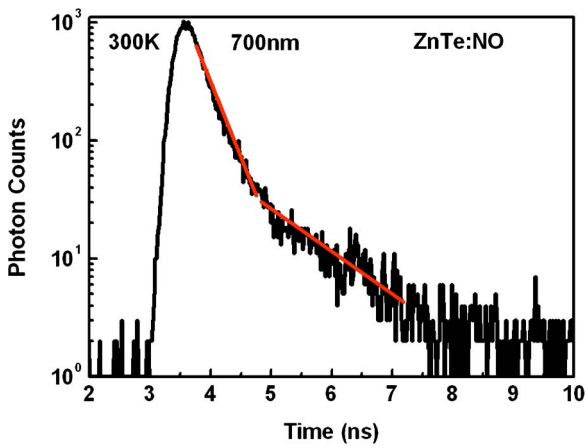


FIG. 2. (Color online) Time-resolved PL of ZnTe:NO at 700 nm.

to the fast radiative recombination rate ($B_0p$) and the Auger recombination rate ($C_0p^2$) in ZnTe material with high p type doping, where the radiative recombination coefficient ($B_0$) is estimated to be $7.1\times10^{-10}$ $cm^3/sec$ (Ref. 21), and the Auger recombination coefficient ($C_0$) is typically about $10^{-29}$ $cm^6/sec$ (Ref. 22). The incorporation of oxygen in the ZnTe:NO sample provides an additional recombination path for photogenerated carriers, resulting in the observed peak centered at 700 nm. The electronic states corresponding to oxygen provide a means to trap electrons from the CB, where the resulting strong emission from the oxygen states demonstrates a significantly longer carrier lifetime due to the nature of the localized oxygen defect. The CB to VB transition disappears for the ZnTe:O sample with a high concentration of oxygen states and no p-type doping, while the transition corresponding to oxygen states increases. This behavior can be explained by fast capture into the high density of oxygen states, in conjunction with reduced CB to VB recombination rates due to reduced hole concentration. The longer carrier lifetime associated with oxygen states in the ZnTe:O sample may be attributed to reduced hole concentration in comparison to the ZnTe:N and ZnTe:NO samples. The carrier populations in the CB, VB, and IB can be expressed by the following rate equations (in the absence of external generation)

$$\frac{dn}{dt} = -\frac{n}{\tau_{CV}} - \frac{n}{\tau_{CI}} - \frac{n}{\tau_{SRH1}}, \tag{1}$$

$$\frac{dN_I}{dt} = \frac{n}{\tau_{CI}} - \frac{N_I}{\tau_{IV}}, \tag{2}$$

$$\frac{dp}{dt} = \frac{dn}{dt} + \frac{dN_I}{dt}, \tag{3}$$

where $n$, $p$, and $N_I$ are the electron density in the CB, hole density in the VB, and electron concentration in the oxygen states, respectively. Radiative recombination is assumed to be the dominant process for this analysis, with the exception of relaxation of carriers from CB to oxygen states. The carrier lifetimes for various transitions are given by the variables $\tau_{CV}$ (CB to VB), $\tau_{IV}$ (IB to VB) and $\tau_{CI}$ (CB to IB) and may be expressed by

$$\tau_{CV} = \frac{1}{B_0(p_0+n_0+\Delta p)} \cong \frac{1}{B_0 p}, \tag{4}$$

$$\tau_{IV} = \frac{1}{B_1(p_0+\Delta p)} \cong \frac{1}{B_1 p}, \tag{5}$$

$$\tau_{CI} = \frac{1}{v_{th}\sigma_n(N_O - N_I)}, \tag{6}$$

where $B_0$ is the radiative recombination coefficient for CB to VB transition in ZnTe, with a value of $7.1\times10^{-10}$ $cm^3/sec$ (Ref. 21). $B_1$ is the radiative recombination coefficient extracted from the power dependent TPRL shown in Fig. 3(b). The electron and hole concentrations $p_0$ and $n_0$ are values under thermal equilibrium, where $\Delta p$ is the injected hole concentration. The equilibrium electron concentration is neglected in the lifetime expressions due to p-type conductivity in all samples. The value of $\tau_{CI}$ is determined using the thermal velocity of electrons at room temperature $v_{th}=2.6$

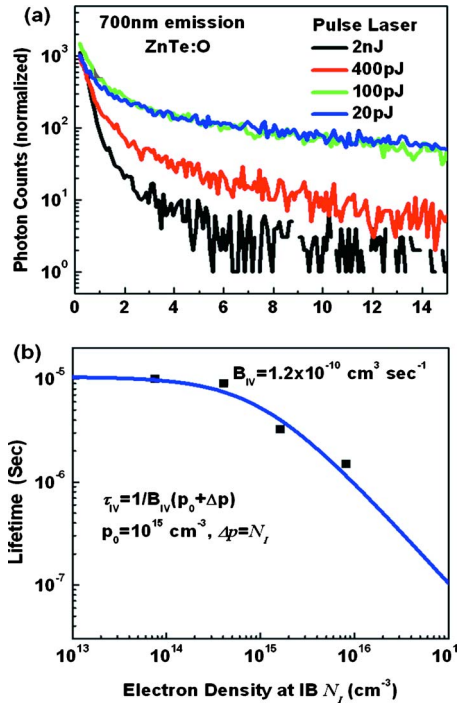


FIG. 3. (Color online) Excitation-dependent TRPL of (a) ZnTe:O at 700 nm and (b) resulting carrier lifetime time constants.

$\times 10^7$ cm/s, concentration of oxygen atoms $N_O$ inferred from absorption measurements, and assuming a capture cross section for electrons of $\sigma_n = 2 \times 10^{-14}$ cm$^2$ (Ref. 16). The injected carrier density may be related to the TRPL excitation conditions assuming the absorption coefficient for ZnTe at 3.1 eV of approximately $\alpha = 1.5 \times 10^4$ cm$^{-1}$ (Ref. 23) and a uniform carrier distribution in the ZnTe layer.

The simulated decay time constants for electrons in the IB under varying excitation are shown in Fig. 4 in good agreement with TRPL measurements. The effective carrier lifetime for electrons in the CB based on simulations of the above rate equations is also shown in Fig. 4 for varying injection density, along with the lifetime of electrons in the IB. Based on these simulations, the effective carrier lifetime for CB electrons show the expected increase with increasing excitation density due to an increase in electron population in IB states. The carrier lifetime for IB electrons also show a corresponding decrease with injection density, though it is still orders of magnitude higher than the lifetime for CB electrons. The dependence of lifetime for CB and IB electrons may be divided into three regions according to injection density relative to the background hole concentration ($10^{15}$ cm$^{-3}$) and IB state density ($10^{18}$ cm$^{-3}$). The effective lifetime of CB electrons may be extended to approximately 1 ns, when the IB states are fully occupied, which would greatly improve the ability to extract carriers generated from a multiphoton process in an IBSC device.

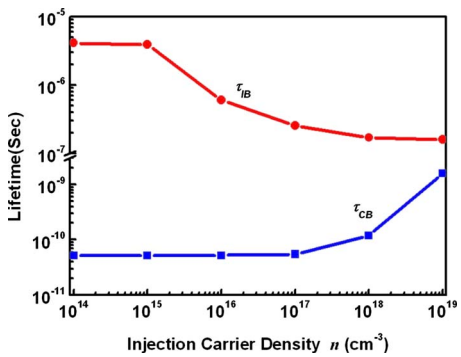


FIG. 4. (Color online) Simulated effective carrier lifetime for electrons at the CB and IB for varying injection.

Long carrier lifetime (>1 $\mu$s) is measured for electrons in oxygen states in ZnTe, where lifetime shows an inverse proportionality with hole density. Shorter carrier lifetime is measured for IB states in p-doped ZnTe:NO and ZnTe:N material where hole population is significantly larger. Short lifetime is observed for electrons in the CB, and is attributed to the fast relaxation of carriers from the CB to IB. Rate equation analysis suggests that the effective lifetime of CB electrons also exhibits a dependence on injected carriers, where increase in lifetime is possible when injection is on the order of the IB state density. High-injection conditions, such as would be present in solar concentrator cells, would serve to enhance the carrier lifetime for CB electrons and resulting conversion efficiency for IBSCs based on these materials.

Material growth was supported by the donors of the American Chemical Society Petroleum Research fund, and optical measurements and analysis at UM were supported by part of the Center for Solar and Thermal Energy Conversion in Complex Materials, an Energy Frontier Research Center funded by the U.S. Department of Energy, Office of Science, Office of Basic Energy Sciences under Award No. DE-SC0000957.

[1] A. Luque and A. Marti, Phys. Rev. Lett. **78**, 5014 (1997).
[2] A. Marti and G. L. Araujo, Sol. Energy Mater. Sol. Cells **43**, 203 (1996).
[3] K. Barnham, B. Braun, J. Nelson, M. Paxman, C. Button, J. S. Roberts, and C. T. Foxon, Appl. Phys. Lett. **59**, 135 (1991).
[4] A. Marti, L. Cuadra, and A. Luque, IEEE Trans. Electron Devices **48**, 2394 (2001).
[5] V. Popescu, G. Bester, M. C. Hanna, A. G. Norman, and A. Zunger, Phys. Rev. B **78**, 205321 (2008).
[6] A. M. Kechiantz, L. M. Kocharyan, and H. M. Kechiyants, Nanotechnology **18**, 405401 (2007).
[7] A. Franceschetti, S. Lany, and G. Bester, Phys. E **41**, 15 (2008).
[8] R. Oshima, A. Takata, and Y. Okada, Appl. Phys. Lett. **93**, 083111 (2008).
[9] A. Luque, A. Marti, C. Stanley, N. Lopez, L. Cuadra, D. Zhou, and A. Mckee, J. Appl. Phys. **96**, 903 (2004).
[10] K. M. Yu, W. Walukiewicz, J. W. Ager, D. Bour, R. Farshchi, O. D. Dubon, S. X. Li, I. D. Sharp, and E. E. Haller, Appl. Phys. Lett. **88**, 092110 (2006).
[11] E. Cánovas, A. Marti, A. Luque, and W. Walukiewicz, Appl. Phys. Lett. **93**, 174109 (2008).
[12] W. M. Wang, A. S. Lin, and J. D. Phillips, Appl. Phys. Lett. **95**, 011103 (2009).
[13] G. Beaucarne, A. S. Brown, M. J. Keevers, R. Corkish, and M. A. Green, Prog. Photovoltaics **10**, 345 (2002).
[14] H. Kasai, T. Sato, and H. Mastsumura, *26th IEEE Photovoltaic Specialists Conferences*, 215, Anaheim, CA, September 29–October 3, 1997 (IEEE, New York, 1997).
[15] A. Lin, W. Wang, and J. Phillips, J. Appl. Phys. **105**, 064512 (2009).
[16] J. D. Cuthbert and D. G. Thomas, Phys. Rev. **154**, 763 (1967).
[17] W. Wang, W. Bowen, S. Lin, S. Spanninga, and J. Phillips, J. Electron. Mater. **38**, 119 (2009).
[18] R. S. Title, G. Mandel, and F. F. Morehead, Phys. Rev. **136**, A300 (1964).
[19] Y. Nabetani, T. Okuno, K. Aoki, T. Kato, T. Matsumoto, and T. Hirari, Phys. Status Solidi A **203**, 2653 (2006).
[20] M. Felici, A. Polimeni, M. Capizzi, Y. Nabetani, T. Okuno, K. Aoki, T. Kato, T. Matsumoto, and T. Hirai, Appl. Phys. Lett. **88**, 101910 (2006).
[21] D. Z. Garbuzov, J. Lumin. **27**, 109 (1982).
[22] U. Strauss and W. W. Ruhle, Appl. Phys. Lett. **62**, 55 (1993).
[23] W. Wang, A. Lin, and J. D. Phillips, J. Electron. Mater. **37**, 1044 (2008).